Hysteresis effect in FePd magnetic stripes studied by coherent soft X-ray resonant magnetic scattering

K. Chesnel,[a,b]* G. van der Laan,[c] F. Livet,[d] G. Beutier,[b] A. Marty,[b] M. Belakhovsky,[b] A. Haznar[c,e] and S. P. Collins[c,f]

[a]ALS, Lawrence Berkeley National Laboratory, 1 Cyclotron Road, Berkeley, CA 94720, USA, [b]DRFMC, CEA-Grenoble, 17 avenue des Martyrs, 38054 Grenoble, France, [c]Magnetic Spectroscopy, Daresbury Laboratory, Warrington WA4 4AD, UK, [d]LTPCM, ENSEEG-Domaine Universitaire, BP 75, 38402 Saint-Martin d'Hères, France, [e]Institute of Low Temperature and Structure Research of the Polish Academy of Sciences, PO Box 1410, Wroclaw, Poland, and [f]Diamond Light Source, Rutherford Appleton Laboratory, Didcot OX11 0QX, UK.
E-mail: kchesnel@lbl.gov

An FePd thin film sample, showing magnetic stripe domains as imaged by magnetic force microscopy, has been measured by soft X-ray resonant magnetic scattering in reflection geometry. Illumination with coherent radiation, produced by inserting a 20 µm pinhole in front of the sample, leads to a magnetic speckle pattern in the scattered intensity that gives access to the domain morphology. Application of an in-plane magnetic field for a few seconds gives a strong change in the observed intensity fluctuations, which indicates a large degree of variation between the two patterns taken before and after field exposure. From the speckle pattern we calculate a degree of coherence of $\beta = 0.5$ for the incident beam.

1. Introduction

X-ray scattering has become a favourite tool for studying the structure of thin films and multilayers, providing the most sensitive and highest resolution data on the interface structure. While these measurements have been applied routinely in the hard X-ray region, only recently have the new possibilities offered by soft X-rays been fully realised (Tonnerre *et al.*, 1996; van der Laan *et al.*, 1999; Kortright & Kim, 2000; Jaouen *et al.*, 2002, 2004). In 3*d* transition metals the excitation of the 2*p* electrons into unoccupied 3*d* states gives strong absorption edges with energies in the soft X-ray region (van der Laan & Thole, 1991). At these energies, resonant scattering causes a huge enhancement of the scattering cross section, as well as element specificity. By using linearly or circularly polarized light the resonant scattering becomes sensitive to the magnetization direction of the specific atoms (Hannon *et al.*, 1988), hence providing the possibility for magnetic contrast. One aspect, however, has remained dormant until recently: the coherence of the X-rays. When coherent light scatters from a random structure, the intensity of the scattered radiation exhibits a pronounced random interference pattern, known as speckle, which contains information on the local configuration of the sample structure. Coherent X-ray beams from third-generation synchrotrons can now be used to study the magnetic correlation in materials at the nanoscopic length scale as demonstrated by several recent experiments (Yakhoo *et al.*, 2001; Peters *et al.*, 2000; Hu *et al.*, 2001; Chesnel *et al.*, 2002; Rahmim *et al.*, 2002; Pierce *et al.*, 2003; Eisebitt *et al.*, 2003; Chesnel, Belakhovsky, Beutier *et al.*, 2004).

To reconstruct the local configuration of coherent illuminated objects from the speckle pattern would require solving the so-called phase problem, which is normally only possible under very favourable circumstances (Miao *et al.*, 1999; Robinson *et al.*, 2001). Such a reconstruction has been achieved using a charge scattering pattern but not yet using a magnetic scattering pattern. Since the magnetization is given by a three-dimensional vector profile, the reconstruction problem is even more complicated than for the charge contribution. An alternative approach consists in performing speckle metrology to measure the statistical evolution of the microscopic magnetic domains under a change of an external parameter such as the applied field. A recent study by Pierce *et al.* (2003) on perpendicular magnetic films, consisting of a CoPt multilayer, shows how to quantify the microscopic magnetic return point memory, by following the evolution of the speckle pattern in an applied magnetic field through the hysteresis loop and after many cycles. Here, we are interested in similar effects in FePd films, but present a very different approach to quantify the speckle pattern – and therefore the magnetic configuration – under evolution of the magnetic field.

In this paper we focus on the micromagnetic processes in FePd alloy thin films which have a high perpendicular magnetocrystalline anisotropy. We have used soft X-ray resonant magnetic scattering to investigate the periodicity of the stripe domains. These materials have some important advantages in the case of a scattering experiment: (i) they are chemically and structurally homogeneous on the length scale of the magnetic domains and, therefore, do not give any additional structural scattering or charge-magnetic interference; (ii) the order (disorder) of the stripe domains can be tailored by varying the growth conditions; and (iii) the X-ray absorption at the Fe L_3 edge is very large and strongly dichroic, giving rise to a huge magnetic resonance enhancement. In the following we will show how coherent X-ray resonant magnetic scattering (CXRMS) allows us to study microscopic changes of the magnetic configuration in these systems. At resonance the scattering pattern displays magnetic peaks, which correspond to the antiferromagnetic ordering of the magnetic domains. Illumination with coherent light produces a speckle pattern that is representative of the local disorder in the stripe configuration. We find that by applying an in-plane magnetic field along the stripe direction for a few seconds there is a dramatic change in the speckle pattern, reflecting a similarly large change in the local domain structure. Furthermore, from the measured patterns we were able to calculate the degree of coherence of the incident beam as well as the degree of variation after applying the field.

The outline is as follows. In §2 we describe the preparation and characterization of the system. In §3 we describe the technique of CXRMS and the specific reflection geometry. The results obtained from an FePd film are discussed in §4. The analysis is developed and discussed in §5. Finally, conclusions are drawn in §6.

2. Description of the system

The system under study is a 40 nm-thick FePd film with strong perpendicular magnetic anisotropy, displaying a striped magnetic domain configuration. We briefly describe the growth conditions and the characterization of the magnetic configuration.

2.1. Epitaxic growth, film structure

The thin film of $Fe_{0.5}Pd_{0.5}$ alloy was grown with molecular beam epitaxy onto a MgO(001) substrate at the Commissariat à l'Energie Atomique (CEA) in Grenoble, France. Epitaxial deposition was

performed at high temperature in order to favour the ordering of the FePd in a $L1_0$ phase, which has an alternation of Fe and Pd atomic planes along the perpendicular axis (growth direction) as illustrated in Fig. 1(a). Such a structure induces a strong perpendicular magnetocrystalline anisotropy, leading to sample magnetization with a large perpendicular component, which breaks up into magnetic stripe domains in order to reduce the stray field energy. Further details about the sample can by found by Gehanno et al. (1997).

2.2. Magnetic force microscopy images

The magnetic stripes can be imaged using magnetic force microscopy (MFM). The image in Fig. 1(b), taken in the remanent state, shows that the stripes are aligned along a specific direction created by prior application of an external magnetic field. The stripe periodicity observed in the image is $\sim$93 nm (i.e. the domain width is $\sim$46.5 nm). The domain structure is driven by the competition between the perpendicular anisotropy and the thin film shape anisotropy (Kittel, 1946) resulting in reverse domains with black and white contrast in the image corresponding to positive and negative magnetization normal to the film surface.

While the MFM technique is sensitive to the magnetic stray fields emerging from the surface, and probes only the perpendicular component of the magnetization, the X-ray resonant magnetic scattering (XRMS) technique is more powerful. X-rays penetrate the film in depth, and polarized X-rays can provide information about the three-dimensional magnetic profile inside the film (van der Laan et al., 2003).

3. Experiment

We describe the experimental set-up, where we use the reflection geometry, leading to specific expressions for the scattering vector. We will also discuss both the longitudinal and transversal coherence of the light together with the sampling conditions.

3.1. Experimental set-up, incidence angle, pinhole, CCD camera

The experiment was performed on the soft X-ray beamline ID08 at the European Synchrotron Radiation Facility (ESRF) using the Daresbury in-vacuum diffractometer (van der Laan, 2001; Roper et al., 2001). Measurements were performed with $99 \pm 1\%$ circularly polarized X-rays near the Fe L_3 absorption edge in order to enhance the magnetic contrast in the scattering process. The experimental set-up is illustrated in Fig. 2(a). The scattering measurements were performed in reflection geometry, at an incidence angle of 22.5° and with two-dimensional detection using a charge-coupled device (CCD) camera mounted at 45° at a distance of 46 cm from the sample. The CCD had an active area of 28 mm $\times$ 26 mm, consisting of 1242 $\times$ 1152 pixels of dimensions 22.5 µm $\times$ 22.5 µm.

In order to obtain a coherent X-ray beam the conditions for both longitudinal and transverse coherence need to be fulfilled (Born & Wolf, 1997). The longitudinal (or temporal) coherence length can be written as $\Lambda_1 = \lambda^2/(2\Delta\lambda)$. Hence, at a given wavelength λ, Λ_1 is determined by the resolving power $\lambda/\Delta\lambda$ of the monochromator, where $\Delta\lambda$ is the spectral width. At the Fe L_3 resonance wavelength of $\lambda = 17.54$ Å (708 eV), $\lambda/\Delta\lambda \simeq 3000$, so that $\Lambda_1 \simeq 3$ µm. The longitudinal coherence length is unimportant when it is large compared with any longitudinal path differences in the diffraction process. Since the absorption lengths in the sample are very small at resonance [$\sim$30 nm in pure Fe (Nakajima et al., 1999)] and the reported measurements are made close to the specular configuration, the condition for longitudinal coherence is largely fulfilled. This would not necessarily be the case off-resonance and for very dilute samples.

Also the transverse coherence length is proportional to λ and in our case this coherence length is $\sim$50 µm. To obtain transverse coherence, a 20 µm pinhole was positioned at 5 cm in front of the sample, as a spatial filter. The distance between the pinhole and the sample is small enough (near field condition) to neglect diffraction
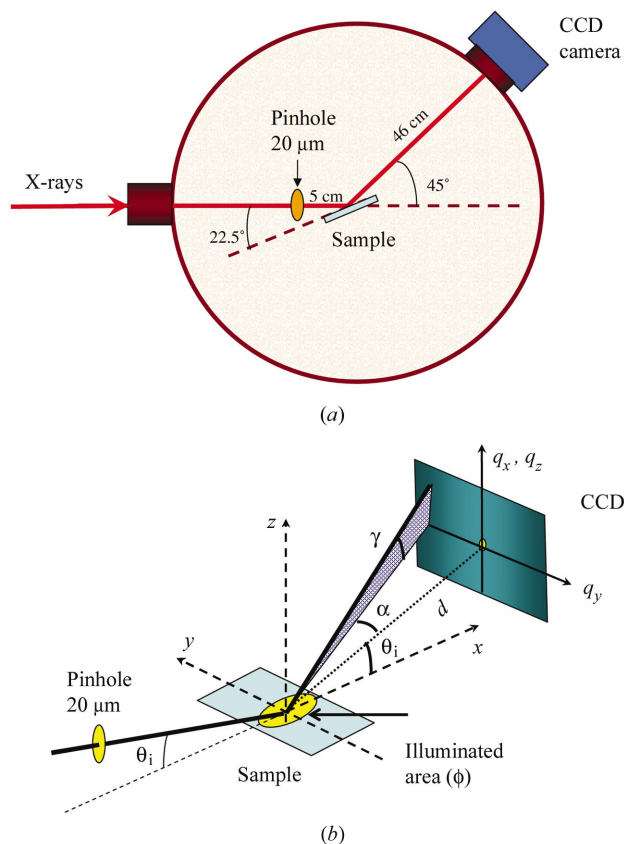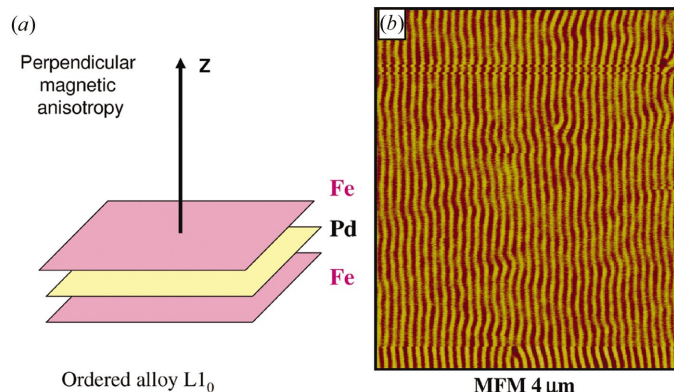

(a)

(a)

(b)

Figure 1
(a) Structure for the FePd alloy in the $L1_0$ phase leading to perpendicular magnetic anisotropy (i.e. normal to the layers). (b) Magnetic force microscopy image measured from the top layer of a 40 nm FePd thin film displaying magnetic stripes, where the perpendicular magnetization component alternates between pointing up and down.

Figure 2
(a) Schematic of the experimental set-up in reflection geometry (in the vertical plane) with two-dimensional detection using a CCD camera. (b) Sketch of the scattering geometry: θ_i corresponds to the incident angle, while α and γ correspond to the horizontal and vertical angular deviation, respectively, of the scattered light with respect to the central specular beam position. The magnetic stripes of the sample are along the x direction (transverse geometry).

effects (Chesnel *et al.*, 2002), so that the illuminated area on the sample surface is roughly the projection of the pinhole aperture, which corresponds to an ellipse whose transversal length (along the short axis) is ∼20 µm and longitudinal length (along the long axis) is ∼52 µm (*cf.* Fig. 2*b*). The sample is positioned with the magnetic stripes parallel to the scattering plane (longitudinal scattering geometry); therefore the coherent illuminated area covers ∼215 magnetic periods (*i.e.* ∼430 magnetic domains).

3.2. Scattering geometry

As shown in Fig. 2(*b*), the direction of scattered light that is recorded on the two-dimensional detector can be indexed by the two angles α and γ, corresponding to the horizontal and vertical angular deviation of the scattered light, respectively, with respect to the central specular beam direction. These angular deviations are proportional to the components of the scattering vector, **q**, along the transverse direction (q_y) and the longitudinal direction (q_x). In the approximation that α and γ are small compared with θ_i, these components are given as

$$
\begin{aligned}
q_x &= k\left[\cos\theta_i - \cos(\theta_i + \gamma)\right] \simeq (k\sin\theta_i)\,\gamma, \\
q_y &= k\sin\alpha \simeq k\alpha, \\
q_z &= k\left[\sin\theta_i + \sin(\theta_i + \gamma)\right] \simeq 2k\,\sin\theta_i,
\end{aligned}
\tag{1}
$$

where $k = 2\pi/\lambda$ is the wavevector at the given wavelength.

These expressions show immediately that the vertical and horizontal directions on the CCD detector (defined by the angles α and γ) are not equivalent concerning the conversion in scattering vector units. In other words, the same variation in q_x and q_y requires a larger angular variation vertically than horizontally by a factor $(\sin\theta_i)^{-1}$. This asymmetry, unique to the reflection geometry, induces an apparent stretching of the scattering pattern in the vertical direction by a factor $(\sin\theta_i)^{-1}$, which is 2.6 in the case of our geometry. Although q_z varies with γ, we can consider the sample as two-dimensional owing to the small absorption length. Therefore, the intensity of the arising speckle rods is expected not to vary significantly in the range of q_z available to the camera.

For both directions we can define a probing length corresponding to the length scale at which the magnetic profile can be probed. From (1) it follows that the relation between a probing length, l_x (l_y), parallel to the sample surface, the corresponding change in the scattering vector component, δq_x (δq_y) and the angular difference, $\delta\gamma$ ($\delta\alpha$), is given as

$$
\begin{aligned}
l_x &= 2\pi/\delta q_x = (1/\sin\theta_i)(\lambda/\delta\gamma), \\
l_y &= 2\pi/\delta q_y = \lambda/\delta\alpha.
\end{aligned}
\tag{2}
$$

Given the CCD pixel size (22.5 µm) and the distance to the detector (460 mm), the opening angle of a single pixel is $\gamma_{\text{pix}} = \alpha_{\text{pix}} = 0.05$ mrad, so that the maximum length that can be resolved is $l_{x(\text{max})} = 90$ µm longitudinally and $l_{y(\text{max})} = 35$ µm transversally. These lengths are longer than the size of the illuminated area in both directions [$l_{x(\text{obj})} \simeq 20$ µm and $l_{y(\text{obj})} \simeq 52$ µm]. In other words, the object is oversampled in each direction, since the oversampling condition is given as

$$
l_{\text{max}}/l_{\text{obj}} > 1.
\tag{3}
$$

When the oversampling factor is larger than unity we measure a speckle pattern, otherwise we measure a configurational average. If needed, the oversampling factor can be increased in several different ways, such as by moving the camera further away from the sample, by using a smaller pixel size (CCD chips with 13 µm × 13 µm are commercially available), by reducing the size of the pinhole, or by

using a 'pinhole' sample [*e.g.* Chesnel *et al.* (2002) used a 8 µm nanostructure FePd wire as the object].

Since the acceptance half-angle for the detector is $\alpha_{\text{max}} = \gamma_{\text{max}} = 30$ mrad ($\sim 1.7°$), the minimum periodicity that can be imaged (using one quadrant of the CCD) is $l_{y(\text{min})} \simeq 60$ nm and $l_{x(\text{min})} \simeq 160$ nm, which gives the ultimate spatial resolution for the sample. Since the FePd stripe domain periodicity is typically 100 nm, which gives $\alpha \simeq 17.5$ mrad ($= 1°$), the spatial resolution is sufficient for magnetic stripes measured in the transverse scattering geometry.

4. Results

4.1. CCD images and speckle pattern

Fig. 3 shows the scattering pattern recorded with the CCD camera at the photon energy of the Fe L_3 resonance edge using circular polarization. The bright central spot corresponds to the specular reflected beam with satellite peaks at both sides. Since the satellite peaks appear only at the resonance energy, they are due to magnetic scattering. Their position with respect to the central peak corresponds to the transverse stripe periodicity of 93 nm, confirming the MFM results. The magnetic peaks show a 'banana' shape, which is only partially due to the vertical stretching of the image as given by (2). The horizontal width of the magnetic peak gives the transversal magnetic correlation length, $l_y \simeq 2$ µm, in the direction perpendicular to the stripes. This length corresponds to roughly 20 magnetic periods, which shows that the alignment of the stripes is rather good. The vertical width of the peak gives the longitudinal magnetic correlation length, $l_x \simeq 700$ nm. This length, which is in the direction of the stripes, gives an indication of the average distance between defects, forks and meandering. In a more general way, the scattering pattern recorded on the CCD camera in the reflection geometry gives an indication of the morphological defects in the two-dimensional magnetic stripe patterns. If the stripes were strictly parallel, with perfect long-range order, we should observe a pure Dirac peak at the position of the satellite. Since the pattern presents defects, we observe scattering spots whose detailed shape is connected to the specific configuration of the magnetic domains.

The difference in intensity of the left and right magnetic peak, shown in Fig. 3, is due to the presence of closure domains, which leads to an interference between the scattering amplitudes from the perpendicular and in-plane magnetized domains (Dürr *et al.*, 1999; van der Laan *et al.*, 2000; Dudzik *et al.*, 2000). Consequently, the peak
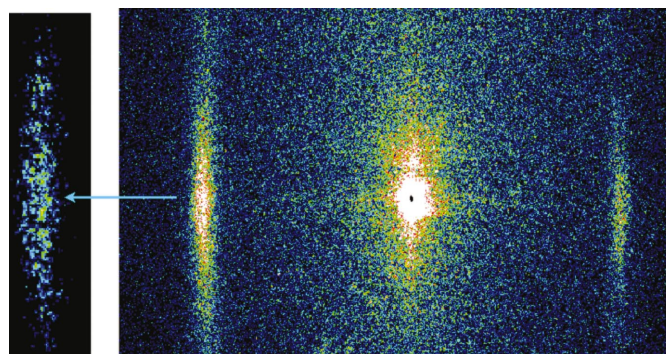

Figure 3
Coherent X-ray resonant magnetic scattering pattern in the region of interest obtained from a 40 nm FePd film at the Fe L_3 edge, in reflection geometry using circularly polarization. The central spot corresponds to the reflected beam, while the left and right satellites correspond to magnetic diffraction peaks due to the stripe periodicity. Left-hand image: enlarged view of the left satellite clearly showing the speckle pattern.

intensities reverse with the light helicity as, for example, seen in the scattering images shown by Chesnel, Belakhovsky, Marty *et al.* (2004).

The enlarged view of the magnetic satellite area in Fig. 3 (left) clearly shows the strong intensity fluctuations. This so-called speckle pattern can only be observed with coherent radiation – here obtained using the pinhole – and is due to the local magnetic configuration of the coherently illuminated sample area. The scattering pattern provides two different kinds of information, namely (i) the global position and width of the magnetic satellite, that is related to the long-range periodicity, and (ii) the speckle pattern, that is related to the short-range order, *i.e.* the magnetic disorder of the domains.

4.2. Evolution of speckle pattern with magnetic field

Fig. 4 shows the evolution of the scattering pattern under an *in situ* external magnetic field, applied along the stripe direction. Fig. 4(a) has been obtained at the remanent state (zero field), while Fig. 4(b) has been measured under a 120 mT in-plane field. The comparison between both patterns shows that the central specular spot and the diffuse intensity are clearly not affected by applying the field, but the intensity of the magnetic satellite becomes much weaker. This indicates that the intensity of the scattering is reduced while applying an in-plane field, because the perpendicular magnetization component (whose periodicity gives rise to the magnetic satellite) is decreased, while the in-plane longitudinal magnetization component (which does not contribute to the periodicity) is increased. There is a critical value of the field beyond which the magnetic satellite disappears because the system has lost its periodic stripe domain configuration and has become a uniform in-plane domain. Furthermore, under applied field the magnetic peak moves slightly further away from the specular spot. This change in the satellite position indicates that the stripe period decreases with magnetic field (Marty *et al.*, 2000). In this case the period of 93 nm at remanence reduced to 91 nm at 120 mT.

4.3. Hysteresis effect (magnetic memory)

Observing the effect of an *in situ* magnetic field on the magnetic speckle pattern raises the question of the reproducibility of the speckle pattern at the remanent state after releasing the field. Would one retrieve the same speckle pattern, and therefore the same magnetic local configuration? In other words, has the system any magnetic memory? Fig. 5 shows the evolution of the speckle pattern with the magnetic history. Figs. 5(a) and 5(b) have been recorded at the remanent state before and after the application of a 120 mT in-plane magnetic field, respectively. The two patterns are visibly different, suggesting that the system did not retrieve exactly the same configuration after releasing the field. In order to verify that this effect is not due to an evolution in time, a third measurement was performed in the same state without modifying any parameters. The resulting pattern, shown in Fig. 5(c), is exactly the same as pattern (b), demonstrating the reproducibility of the measurement in time and evidencing that the variation between the patterns (a) and (b) is only due to the application of the magnetic field.

5. Analysis

In order to estimate the magnetic memory of the sample, we need to quantify the variation of the speckle pattern. One way to do this is to evaluate the 'degree of variation' between the two patterns (a) and (b) in Fig. 5 and to compare this with the 'degree of coherence' in the first pattern.

5.1. Estimation of the degree of coherence β

From an anisotropic smoothing of the measured speckle intensity, $I(q)$, in Fig. 6(a) we can obtain the spatial average, $I_{inc}(q)$, shown in Fig. 6(b), which corresponds to the intensity that would be obtained using incoherent radiation (Abernathy *et al.*, 1998; Livet *et al.*, 2000). The degree of coherence β is given by the mean square difference between $I(q)$ and $I_{inc}(q)$. The quantity β is evaluated by averaging this squared difference over a chosen surface S, which in our case
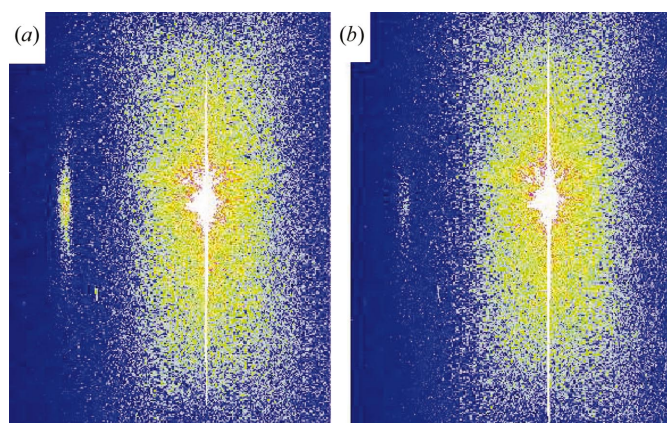

Figure 4
Evolution of the scattering pattern in the region of interest with magnetic field (a) at zero field (remanent state) and (b) under 120 mT in-plane applied magnetic field.
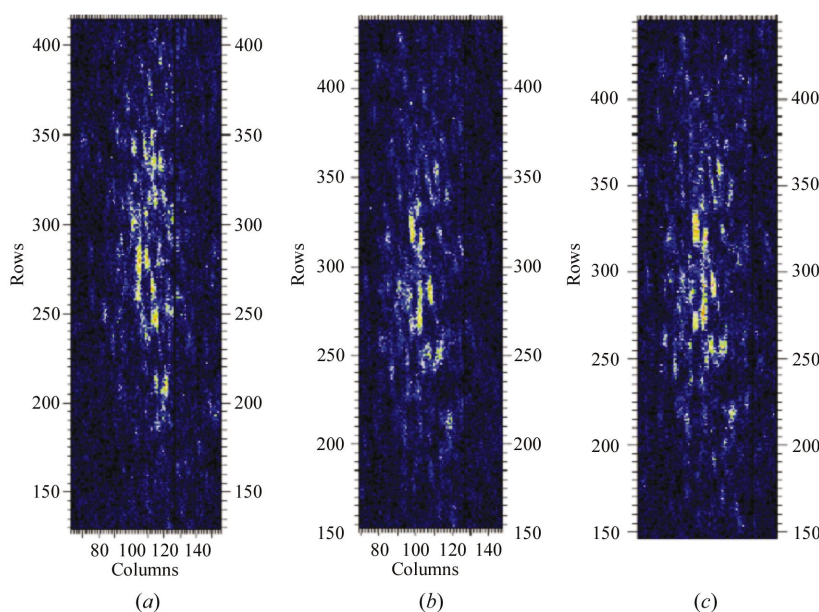

Figure 5
Effect of the magnetic history on the magnetic speckle pattern (a) in initial remanent state, (b) after application of a 120 mT field applied along the stripe direction for a few seconds, (c) repetition of the measurement in (b) without applying a field.

corresponds to the area of the magnetic satellite. By taking the Poisson noise into account, this corresponds to

$$\beta = \frac{\langle [I(q) - I_{\text{inc}}(q)]^2 - I_{\text{inc}}(q) \rangle_S}{\langle [I_{\text{inc}}(q)]^2 \rangle_S}. \quad (4)$$

The speckle pattern in Fig. 6(a) gives a degree of coherence $\beta = 0.5$ (i.e. 50%), confirming the strong contrast in the speckle intensity. Fig. 6(c) shows the measured intensity profile $I(q)$ (intensity of individual pixels connected by a thin line) along a vertical direction across the image of the magnetic peak, which is compared with $I_{\text{inc}}(q)$ (thick line). The fact that each individual speckle in the graph covers slightly more than one pixel demonstrates that the object is indeed oversampled (by a factor of 1.7).

5.2. Degree of variation α

The degree of variation α corresponds to the mean square difference between the intensity of the two patterns Fig. 5(a) and Fig. 5(b). The difference is calculated at each pixel q and averaged over the area S, after correction by the Poisson statistical noise of both images. The result is then normalized as
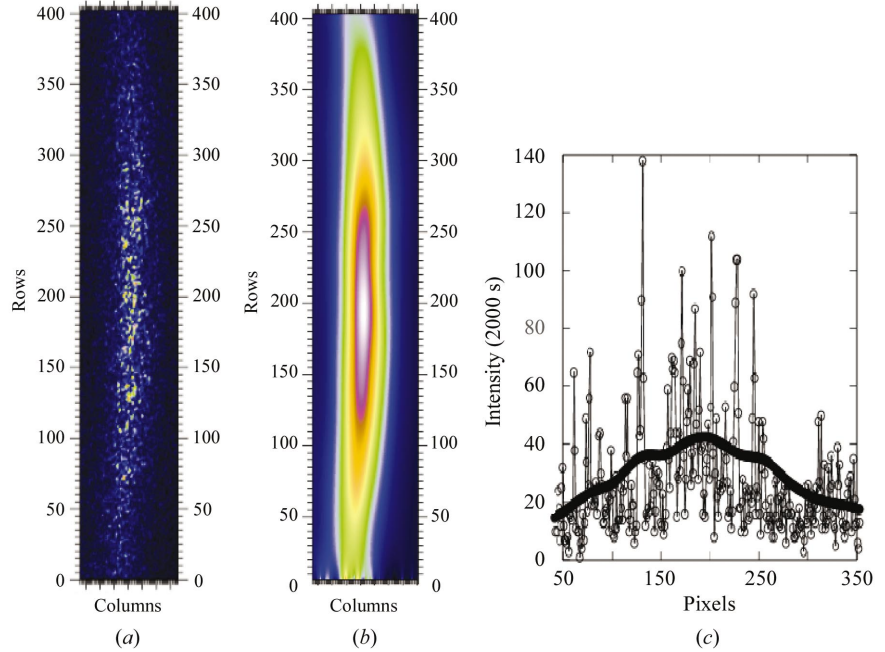

Figure 6
Evaluation of the degree of coherence for the magnetic satellite. (a) Speckle pattern intensity $I(q)$ in the area S of the magnetic satellite. (b) Result of the anisotropic smoothing of the speckle pattern, giving $I_{\text{inc}}(q)$, which corresponds to the intensity that would be obtained using incoherent radiation. (c) Cross section along a vertical line showing the measured intensity $I(q)$ (pixel points connected by the thin line) and $I_{\text{inc}}(q)$ (thick smooth curve), from which the degree of coherence (over S) is calculated as $\beta = 0.5 \pm 0.05$.

$$\alpha = \frac{1}{2} \frac{\langle [I_a(q) - I_b(q)]^2 - [I_{a,\text{inc}}(q) + I_{b,\text{inc}}(q)] \rangle_S}{\langle [I_m(q)]^2 \rangle_S}, \quad (5)$$

where $I_m(q) = \frac{1}{2}[I_{a,\text{inc}}(q) + I_{b,\text{inc}}(q)]$ represents the mean incoherent intensity of the two patterns at each pixel. Since the incoherent part of the scattering patterns Fig. 5(a) and Fig. 5(b) are the same – because both images are obtained at the same macroscopic magnetic point (here the remanent point) – we can assume that $I_{a,\text{inc}}(q) = I_{b,\text{inc}}(q)$ and rename this quantity $I_{\text{inc}}(q)$. Furthermore, we can introduce the quantities $\delta I_a(q) = I_a(q) - I_{\text{inc}}(q)$ and $\delta I_b(q) = I_b(q) - I_{\text{inc}}(q)$ and replace the difference $I_a(q) - I_b(q)$ by $\delta I_a(q) - \delta I_b(q)$ in the expression of α, which becomes

$$\alpha = \frac{1}{2} \frac{\langle [\delta I_a(q) - \delta I_b(q)]^2 - 2I_{\text{inc}}(q) \rangle_S}{\langle [I_m(q)]^2 \rangle_S}. \quad (6)$$

By developing this expression, one obtains

$$\alpha = \frac{1}{2} \frac{\langle [\delta I_a(q)]^2 - I_{\text{inc}}(q) \rangle_S + \langle [\delta I_b(q)]^2 - I_{\text{inc}}(q) \rangle_S}{\langle [I_m(q)]^2 \rangle_S} - \frac{\langle \delta I_a(q) \delta I_b(q) \rangle_S}{\langle [I_m(q)]^2 \rangle_S}. \quad (7)$$

The first two terms in the numerator give independently an estimate of the degree of coherence for the patterns Fig. 5(a) and Fig. 5(b). Since both images have the same degree of coherence β, we can finally connect the coefficient α to the coefficient β as

$$\alpha = \beta - \frac{\langle \delta I_a(q) \delta I_b(q) \rangle_S}{\langle [I_m(q)]^2 \rangle_S}. \quad (8)$$

This expression evidences that the quantity α is a real number that can vary between 0 and its maximal value β. The term $\langle \delta I_a(q) \delta I_b(q) \rangle_S$ represent the coverage between the two speckle patterns Fig. 5(a) and Fig. 5(b). If the two patterns are identical, the coverage is full, then the a and b intensities differ only by the Poisson noise and the

degree of variation is nil ($\alpha = 0$). If the two pattern are completely independent, the coverage is nil and the degree of variation is maximal ($\alpha = \beta$).

Using (8) we obtain a degree of variation of $\alpha = 0.3$ between patterns (a) and (b) in Fig. 5. This result confirms that both patterns are different, but the fact that this value is still smaller than β also indicates that the magnetic pattern is not completely different and has partially kept its initial configuration, i.e. this system presents a significant magnetic memory, at least after application of an intermediate-size magnetic field (smaller than the saturation field).

5.3. Discussion

We show here how to quantify the modifications in the magnetic configuration by estimating the degree of coherence in the speckle patterns and the degree of variation between two images recorded at different stages of the magnetic evolution. This approach can be compared with the analysis developed by Pierce et al. (2003), who present another method to quantify the microscopic changes – and particularly the return point magnetic memory – in magnetic domains. The comparison can be made regarding two specific aspects.

Firstly, in our approach we put an emphasis on quantifying the degree of coherence β that can be derived from the speckle patterns. Under given experimental conditions, all the recorded images will obviously have the same degree of coherence, related to the speckle contrast in the patterns. This degree of coherence provides important information about the quality of the data, that can be a limiting factor in the subsequent analysis, especially when a comparison is made between two different speckle patterns. Unfortunately, this aspect is not discussed at all by Pierce et al. (2003).

Secondly, we introduced a degree of variation α in order to compare two speckle patterns obtained at different stages of the magnetic evolution. This quantity is a real number that can vary

between 0 and β. The fact that the maximum value for α is actually β (and not 1) shows how the quality of the speckle pattern can limit the interpretation of results. Indeed, while a degree of variation equal to 0 means that there is no variation between the two patterns (therefore the magnetic configuration is exactly the same), a degree of variation equal to β (the maximal possible value) means that the two patterns are completely different, as far as the speckle pattern allows to observe such differences (we would like to emphasize this last aspect). In other words, the speckle pattern produced in a coherent scattering experiment provides information about the local magnetic domain structure with a certain resolution that is determined by the experimental conditions (coherence of the light, oversampling conditions etc.). The better the coherence and oversampling conditions are, the more information one can extract from the speckle pattern and the better the sensitivity will be for small changes in the magnetic configuration. If the experimental conditions are in some way deteriorated, so that the coherence is lost, then the degree of coherence becomes close to 0 and the possibility to observe any change in the magnetic domain configuration becomes very limited.

Indeed, under poor coherence conditions the pattern is more likely to be an incoherent scattering pattern and the speckle aspect is lost. In this extreme case, any particular small local change in the magnetic configuration cannot be monitored since the global shape of the scattering pattern remains the same and is related to the averaged domain periodicity but not to the local domain structure. The estimation of the degree of coherence is, therefore, an extremely important step, which should be taken into account before any further analysis of the speckle metrology experiment. This aspect was not considered by Pierce et al. (2003), who developed an analysis based on cross-correlation between speckle patterns. In their analysis, the result of the correlation is quantified by a parameter ρ that can vary from 0 to 1, whatever the quality of the speckle pattern. A degree of correlation $\rho = 0$ evidences that the two compared patterns are completely different, whereas if $\rho = 1$ it means that the two patterns are exactly the same. Incidentally, the authors use the coefficient ρ to quantify the magnetic memory as the in situ magnetic field is cycled. When under those specific experimental conditions the coherence of the incident light and the oversampling conditions are not optimal, the results of their analysis may be overestimated. In other words it is easier to conclude that two speckle patterns are the same with poor coherence and poor oversampling than with a higher degree of coherence, since not all the details of the pure coherent scattering pattern can be seen with partially coherent light. Therefore we emphasize the importance of quantifying the degree of coherence before performing a pattern comparison, since it can limit the quality of the speckle metrology results.

6. Conclusion

Using coherent soft X-ray resonant magnetic scattering from an FePd thin film sample with magnetic stripe domains we observed strong intensity fluctuations in the magnetic satellites. The speckle pattern was observed with coherent radiation – obtained using a pinhole – and gives information about the local and non-averaged magnetic configuration of the coherent illuminated sample area. While the conventional scattering pattern provides the global position and width of the magnetic satellite, which are related to the long-range periodicity, the speckle pattern is related to the short-range order, i.e. the magnetic disorder of the domains. The obtained speckle pattern corresponds to a degree of coherence for the incident X-rays of $\beta = 0.5$.

The fact that scattering is a photon-in–photon-out technique allows us to study reversal processes under applied magnetic field. After applying an in-plane magnetic field for a few seconds we observed a strong change in the speckle pattern. A 120 mT field gave a degree of variation of $\alpha = 0.3$. Although this is much larger than zero, it is still much smaller than β, indicating a significant magnetic memory effect. This new technique clearly holds great promise for the future of magnetic scattering, with imaging of dynamical disorder among the possibilities.

It is interesting to remark that the experiment has benefited in several ways from the advantages of the soft X-ray region compared with the hard X-rays (van der Laan, 2004). (i) Both the longitudinal and the transverse coherence lengths are proportional to the wavelength λ of the X-rays, so that the coherence flux increases as λ^2, becoming more favourable at longer wavelength. Moreover, owing to the strong absorption for the soft X-ray resonances, the longitudinal coherence length will be much larger than the absorption length. (ii) The long wavelengths of the soft X-rays allow us to access the nanoscopic length scale of the magnetic domain structures. Such length scales are also ideal from the point of view of oversampling, since the diffraction is no longer comprised of sharp Bragg peaks, but of a complicated intensity distribution centred at reciprocal lattice points. In our geometry we covered the transverse (in-plane) length scale 60 nm to 35 µm, where the first value gives the lower limit of the domain periodicity and the second value gives the upper limit of the object size. The three orders of magnitude for the length scale is determined by the total number of pixels in the CCD. (iii) The huge magnetic dichroism for the transition metal $2p \rightarrow 3d$ transitions in the soft X-ray region makes the magnetic scattering much easier to detect. The main price to pay for all these advantages is that the experiments need to be performed under vacuum in order to avoid the absorption of the soft X-rays by air.

References

Abernathy, D. L., Grübel, G., Brauer, S., McNulty, I., Stephenson, G. B., Mochrie, S. G. J., Sandy, A. R., Mulders, N. & Sutton, M. (1998). J. Synchrotron Rad. 5, 37–47.
Born, M. & Wolf, E. (1997). Principles of Optics, 6th ed., ch. X. Cambridge University Press.
Chesnel, K., Belakhovsky, M., Beutier, G., Marty, A., Livet, F., van der Laan, G., Collins, S. P. & Haznar, A. (2004). Phys. Rev. B, 70. In the press.
Chesnel, K., Belakhovsky, M., Livet, F., Collins, S. P., van der Laan, G., Dhesi, S. S., Attané, J. P. & Marty, A. (2002). Phys. Rev. B, 66, 172404/1–4.
Chesnel, K., Belakhovsky, M., Marty, A., Beutier, G., van der Laan, G. & Collins, S.P. (2004). Physica B, 345, 148–152.
Dudzik, E., Dhesi, S. S., Dürr, H. A., Collins, S. P., Roper, M. D., van der Laan, G., Chesnel, K., Belakhovsky, M., Marty, A. & Samson, Y. (2000). Phys. Rev. B, 62, 5779–5785.
Dürr, H. A., Dudzik, E., Dhesi, S. S., Goedkoop, J. B., van der Laan, G., Belakhovsky, M., Mocuta, C., Marty, A. & Samson, Y. (1999). Science, 284, 2166–2168.
Eisebitt, S., Lorgen, M., Eberhardt, W., Luning, J., Stohr, J., Rettner, C. T., Hellwig, O., Fullerton, E. E. & Denbeaux, G. (2003). Phys. Rev. B, 68, 104419/1–6.
Gehanno, V., Marty, A., Gilles, B. & Samson, Y. (1997). Phys. Rev. B, 55, 12552–12555.
Hannon, J. P., Trammell, G. T., Blume, M. & Gibbs, D. (1988). Phys. Rev. Lett. 61, 1245–1248.

Hu, B., Geissbuhler, P., Sorensen, L., Kevan, S. D., Kortright, J. B. & Fullerton, E. E. (2001). *Synchrotron Rad. News*, **14**, 11–19.

Jaouen, N., Tonnerre, J.-M., Raoux, D., Bontempi, E., Ortega L., Muenzenberg, M., Felsch, W., Rogalev, A., Dürr, H. A., Dudzik, E., van der Laan, G., Suzuki, M. & Maruyama, H. (2002). *Phys. Rev. B*, **66**, 134420/1–14.

Jaouen, N., van der Laan, G., Johal, T. K., Wilhelm, F., Rogalev, A., Mylonas, S. & Ortega, L. (2004). *Phys. Rev. B*, **70**. In the press.

Kittel, C. (1946). *Phys. Rev.* **70**, 965–971.

Kortright, J. B. & Kim, S.-K. (2000). *Phys. Rev. B*, **62**, 12216–12228.

Laan, G. van der (2001). *Synchrotron Rad. News*, **14**, 32–36.

Laan, G. van der (2004). *Physica B*, **345**, 137–142.

Laan, G. van der, Chesnel, K., Belakhovsky, M., Marty, A., Livet, F., Collins, S. P., Dudzik, E., Haznar, A. & Attané J. P. (2003). *Superlattices Microstruct.* **34**, 107–126.

Laan, G. van der, Dudzik, E., Collins, S. P., Dhesi, S. S., Dürr, H. A., Belakhovsky, M., Chesnel, K., Marty, A., Samson, Y. & Gilles, B. (2000). *Physica B*, **283**, 171–174.

Laan, G. van der, Dürr, H. A., Dudzik, E., Roper, M. D., Collins, S. P., Hase, T. P. A. & Pape, I. (1999). *Synchrotron Rad. News*, **12**, 5–9.

Laan, G. van der & Thole, B. T. (1991). *Phys. Rev. B*, **43**, 13401–13411.

Livet, F., Bley, F., Mainville, J., Sutton, M., Caudron, R., Mochrie, S. G. J., Geissler, E., Dolino, G., Abernathy, D. L. & Grubel, G. (2000). *Nucl. Instrum. Methods A*, **451**, 596–609.

Marty, A., Samson, Y., Gilles, B., Belakhovsky, M., Dudzik, E., Dürr, H. A., Dhesi, S. S., van der Laan, G. & Goedkoop, J. B. (2000). *J. Appl. Phys.* **87**, 5472–5474.

Miao, J., Charalambous, P., Kirz, J. & Sayre, D. (1999). *Nature (London)*, **400**, 342–344.

Nakajima, R., Stöhr, J. & Idzerda, Y. U. (1999). *Phys. Rev. B*, **59**, 6421–6429.

Peters, J. F., de Vries, M. A., Miguel, J., Toulemonde, O. & Goedkoop, J. B. (2000). *ESRF Newsl.* **32**, 15–16.

Pierce, M. S., Moore, R. G., Sorensen, L. B., Kevan, S. D., Hellwig, O., Fullerton, E. E. & Kortright, J. B. (2003). *Phys. Rev. Lett.* **90**, 175502/1–4.

Rahmim, A., Tixier, S., Tiedje, T., Eisebitt, S., Lörgen, M., Scherer, R., Eberhardt, W., Lüning, J. & Scholl, A. (2002). *Phys. Rev. B*, **65**, 235421/1–13.

Robinson, I. K., Vartanyants, I. A., Williams, G. J., Pfeifer, M. A. & Pitney, J. A. (2001). *Phys. Rev. Lett.* **87**, 195505/1–4.

Roper, M. D., van der Laan, G., Dürr, H. A., Dudzik, E., Collins, S. P., Miller, M. C. & Thompson S. P. (2001). *Nucl. Instrum. Methods A*, **467**, 1101–1104.

Tonnerre, J.-M. (1996). *X-ray Magnetic Scattering* in *Magnetism and Synchrotron Radiation*, edited by E. Beaurepaire, B. Carrière & J.-P. Kappler, pp. 245–273. Les Éditions de Physique, Les Ulis.

Yakhoo, F., Létoublon, A., Livet, F., de Boisieu, M. & Bley, F. (2001). *J. Magn. Magn. Mater.* **233**, 119–122.